Annals of Nuclear Medicine Vol. 14, No. 4, 271–277, 2000

Phantom study of fusion image of CT and SPECT with body-contour generated from external Compton scatter sources

Kazuyoshi SUGA, Naofumi MATSUNAGA, Yasuhiko KAWAKAMI and Mataichi FURUKAWA

Department of Radiology, Yamaguchi University School of Medicine

Purpose: A phantom study was conducted to evaluate the feasibility of body contour definition with Compton scatter photons from extemal sources of technetium-99m pertechnetate (Tc-99m) to create a fusion image of CT and SPECT images.

Methods: External sources of 1 mCi (37 MBq) Tc-99m were placed on each collimator, and body-contour SPECT images were obtained with an energy window of 100 keV ± 25% for detecting 90° and 180° Compton scatter photons of Tc-99m from the body surface in water-filled cylindrical and hexagonal phantoms, and in a chest phantom with a Tc-99m-avid simulated lung nodule and multimethod surface markers. In the chest phantom, each transaxial SPECT slices was registered with the corresponding CT slice by using image-matching soft ware. A summation of the registered images yielded a three-dimensional (3-D) fusion image of this phantom.

Results: This method clearly visualized the body contour on all the SPECT slices in all the phantoms except for the complex hexagonal phantom. There was no significant difference between the known and SPECT-measured diameters of the cylindrical phantom. The fit of CT and SPECT images of the chest phantom was achieved with a mean alignment error of 5% in visual inspection, which was improved to 0.2% after correction of the magnification of the SPECT images according to the resultant dimensional differences. The 3-D fusion image of this phantom effectively visualized the anatomic location of the lung nodule and surface markers.

Conclusion: This simple method effectively provided boundary information on the cold phantoms. Although further improvements in the registration technique with CT images are desirable, the body-contour SPECT image obtained by this method has the potential for accurately creating a 3-D fusion image with CT images, and is a feasible way of anticipating the anatomical localization of a target tissue.

Key words: SPECT, image fusion, Compton scattered photons, body-contour definition

INTRODUCTION

SINGLE PHOTON EMISSION COMPUTED TOMOGRAPHY (SPECT) and X-ray computed tomography (CT) offer complementary information on function and morphology. A fusion of SPECT and CT images provides significant additional information compared to that from each of these images alone, and is an important tool in clinical diagnosis, surgery and therapy. To create a fusion image from these images, accurate definition of body contours of the object in the SPECT imaging is important. The body contour of an object in SPECT images can be determined with object emission data, either from the photopeak[1–3] or Compton scatter windows,[4] 90° or backscatter Compton scatter photons from external sources,[5–8] surface markers,[9,10] and transmission SPECT data.[11–15] Of these methods, the use of Compton scatter photons from external sources may be the simplest and most practical for routine SPECT studies, and could be available for creating a fusion image of SPECT and CT images. This report details a phantom study conducted to experimentally evaluate the feasibility of this method in creating a fusion image with SPECT and CT.

Received February 28, 2000, revision accepted May 18, 2000.

For reprint contact: Naofumi Matsunaga, M.D., Department of Radiology, Yamaguchi University School of Medicine, 1–1–1 Minamikogushi, Ube, Yamaguchi 755–8505, JAPAN.

MATERIAL AND METHODS

Image Acquisition of the Phantoms

To evaluate the accuracy of body contour definition with Compton scatter photons from external sources of technetium-99m (Tc-99m), a simple, cylindrical pharntom with a 9.5-cm inside diameter and a 21-cm length, and a more complicated, hexagonal phantom with a 24-cm inside maximal diameter and a 19.5-cm length were initially studied (Figs. 1–3). Two external sources (1-m*l* syringes filled to 0.1 m*l*) each containing 1 mCi (37 MBq) Tc-99m were first placed directly on the collimators, one per collimator, just outside the field of view of the camera (Fig. 1). The syringes were oriented parallel to the axis of rotation and were symmetrically placed at opposite lateral ends of the two collimators, that is, one syringe was placed to the far right on the upper collimator and the second syringe was placed to the far left on the lower collimator. The phantoms were filled with water, and a SPECT scan was done with a dual-headed camera system (GE, Maxxus 4000-I) fitted with low-energy, high-resolution collimators and interfaced to a computer. An energy window was set at 100 keV ± 25% to mainly detect 110 keV energy of the 90° scatter from the Tc-99m sources and 90 keV energy of the 180° backscatter, although this window also detected some variably-directed Compton scatters. Data were then acquired in a 128 × 128 image matrix for 32 projections over 180° for each camera head (a total of 64 projections over 360°). The acquisition time was 20 sec per projection in the auto rotation mode. The raw data were reconstructed to sequential 32 frame transaxial planes by filtered backprojection with an eight order Butterworth window with an empirically chosen cutoff level of 0.6 cycles/cm. The reconstructed slices were one voxel thick (2.7 mm).

A custom-made chest phantom with 27.5-cm long and with a maximum height of 15-cm was used for three-dimensional fusion imaging of SPECT and CT images (Fig. 4A). This phantom had a body-contour similar to the human chest wall with various circumferences ranging from 62 cm to 78 cm, and the inside of the phantom contained a simulated mediastinal structure surrounded by a simulated lung structure filled with small styrene foam balls. A simulated spherical lung nodule, 50 mm in diameter, was also placed within the simulated lung structure. Radionuclide solution could be poured into this simulated nodule through two-way silicon tubes (Fig. 4-A). The chest phantom was also filled with water, and the simulated lung nodule was filled with 150 μCi (5.55 MBq) of Tc-99m. In addition, as landmarks to evaluate the accuracy of the fit of the CT and SPECT fusion images of this phantom, five commercially available surface markers (multimethod X-ray markers: MM-3003, IZM Medical Products), each filled with 50 μCi (1.85 MBq) of Tc-99m, were randomly placed on the phantom surface (Fig. 4A). These surface markers were not used as the landmarks to register the SPECT and CT images of this phantom. SPECT images were obtained with a three-headed SPECT system (GCA9300 A/H, Toshiba Medical). Three external sources (1-m*l* syringes filled to 0.1 m*l*) each containing 1 mCi (37 MBq) Tc-99m were symmetrically and directly placed on each of the three collimators, as described previously (Fig. 1). SPECT data were acquired in a 128 × 128 image matrix for 18 projections over 120° for each camera head (a total of 64 projections over 360°). The acquisition time was 20 sec

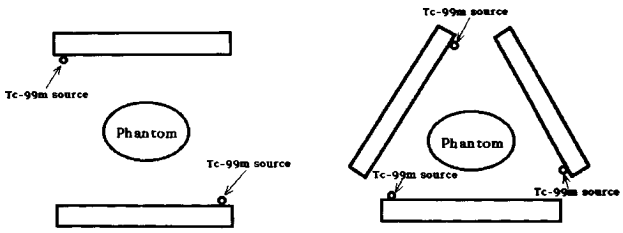

Fig. 1 Schematic illustration of geometric arrangements of the detectors and Tc-99m sources for SPECT image acquisition of the cold phantoms.

Table 1 Comparison of CT and SPECT chest phantom dimensions

Point no.	CT dimension (mm)	SPECT dimension (mm)	difference (mm)
1	100.3	103.6	3.3
2	99.9	110.1	10.2
3	100.3	112.1	12.1
4	70.6	72.4	1.8
5	71.2	70.8	−0.4
6	70.6	71.0	0.4
7	141.2	150.1	8.9
8	140.6	150.3	9.7
9	141.2	149.6	8.4
10	146.5	159.2	12.7
11	145.8	156.6	10.8
12	145.8	152.7	6.9
13	147.8	152.5	4.7
14	74.6	79.6	5.0
15	73.0	78.1	7.1
16	72.9	74.0	5.1
17	73.1	77.2	4.1
18	74.8	79.0	4.2
19	73.9	76.2	2.3
20	74.6	79.2	4.6
21	74.6	78.8	4.2

All dimension comparisons were obtained using anatomically comparable transaxial slices. 1–5: Distance between the surface marker and the phantom center. 6–13: Distance between the surface marker and the basement line. 14: Distance between the central point of the simulated lung nodule and the phantom center. 15–16: Distance between the different peripheral points of the simulated lung nodule and the phantom center

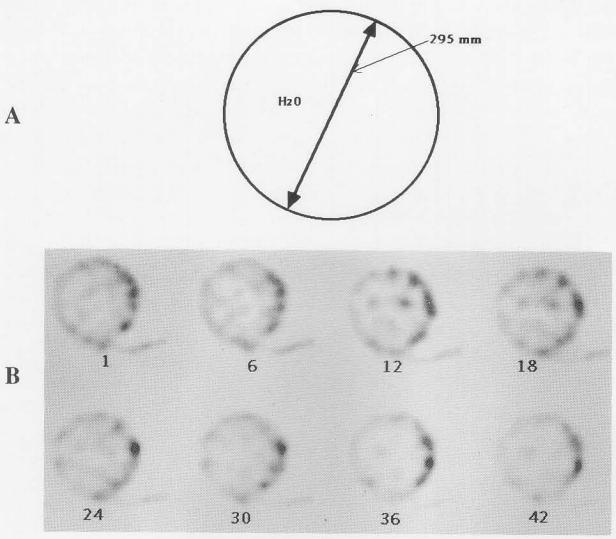

Fig. 2 (A) Schematic illustration of the transverse section of a 290-mm-diameter cylindrical phantom filled with water. (B) One-voxel thick (2.4 mm) transaxial sections of this phantom obtained with reconstruction of the Compton scattered events from two external Tc-99m sources. The body-contour of this phantom is clearly visualized on all the contiguous transverse section images.

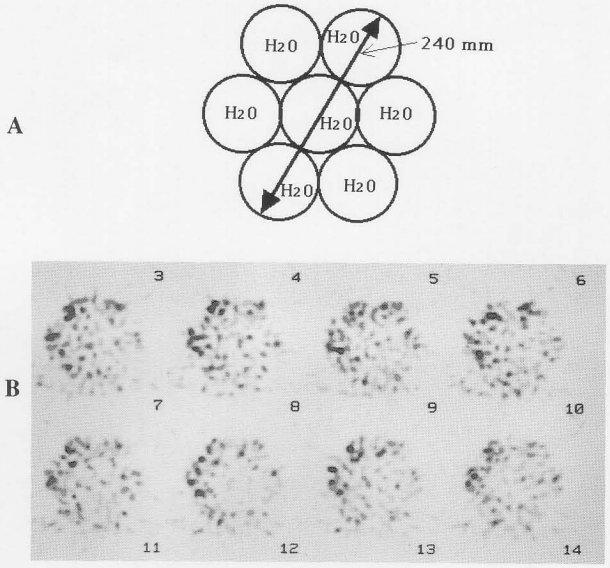

Fig. 3 (A) Schematic illustration of the transverse section of a hexagonal phantom filled with water. (B) One-voxel-thick (2.7 mm) transaxial sections of this phantom obtained with reconstruction of the Compton scattered events from two external Tc-99m sources. The complicated body-contour of this phantom is only fairly visualized.

per projection in the auto rotation mode. Reconstruction of transaxial planes was done in the same way as in the cylindrical phantom, but with a reconstructed slice thickness of 3.2 mm.

Image Fusion of the Chest Phantom

The chest phantom with surface markers was used for CT imaging after it was cleaned of radioactivity. The sequential 42 frame transaxial CT images of the entire phantom were obtained in a 512 × 512 image matrix, with a spiral CT system (Somatom Plus 4). CT scanning was done with a section interval of 3 mm, which approximately matched the SPECT section thickness. The reconstructed SPECT images and CT images of the chest phantom were transferred to a Macintosh computer (Apple Computer Co., USA) through a direct link with the CT and SPECT units. To minimize differences in image geometry, standard bilinear interpolation was used to convert both the CT and SPECT images to the same 256 × 256-matrix format. Corresponding transverse SPECT and CT slices of the chest phantom were selected from the same cranio-caudal level after comparison of the appropriate SPECT coronal image with CT scout view images. Transaxial SPECT and CT images were appropriately windowed, and simultaneously displayed side by side, and were then normalized to allow subsequent simultaneous display. Each of the selected CT and SPECT set slices was then coregistered with commercially available software (IPLab Spectrum, Version 3, Image and measurement Co.) (Fig. 4B). Five or six landmarks of the Compton scatter-generated body contour were selected on the CT and SPECT set slices, and SPECT images were mapped onto the CT images. By applying linear regression techniques to the complete set of landmarked pairs, the errors inherent in each individual landmark pair could be corrected in a least squares sense (i.e., by averaging over the whole set of landmarks). The mapping algorithm used involved standard two-dimensional scaling, translation, rotation, and stretching transformation, so that each point in the SPECT image was shifted uniformly and discretely into registration with the corresponding point on CT images, and fusion images were obtained. Individualized color scales were assigned to each image, and background and saturation values were optimized to facilitate tracer activity visualization of the external marker and simulated lung nodule. Finally, these registered CT-SPECT planes were reconstructed to a three-dimensional, volume-rendered fusion image in a 256 × 256 image matrix, with commercially available reconstruction software (Voxblast, Veytek Inc.) (Fig. 4C).

Evaluation of SPECT Dimensions

To validate the body-contour dimension measurements, the diameters of 10 transaxial SPECT sections of the cylindrical and hexagonal phantoms acquired by the dual-headed camera were measured by multiplying the number of pixels in that distance with a 0.96 cm/pixel calibration factor (1 pixel = 0.96 cm, on the SPECT image transferred to the Macintosh computer), and comparing this with the known inside diameter of the phantom. To quantify the

A

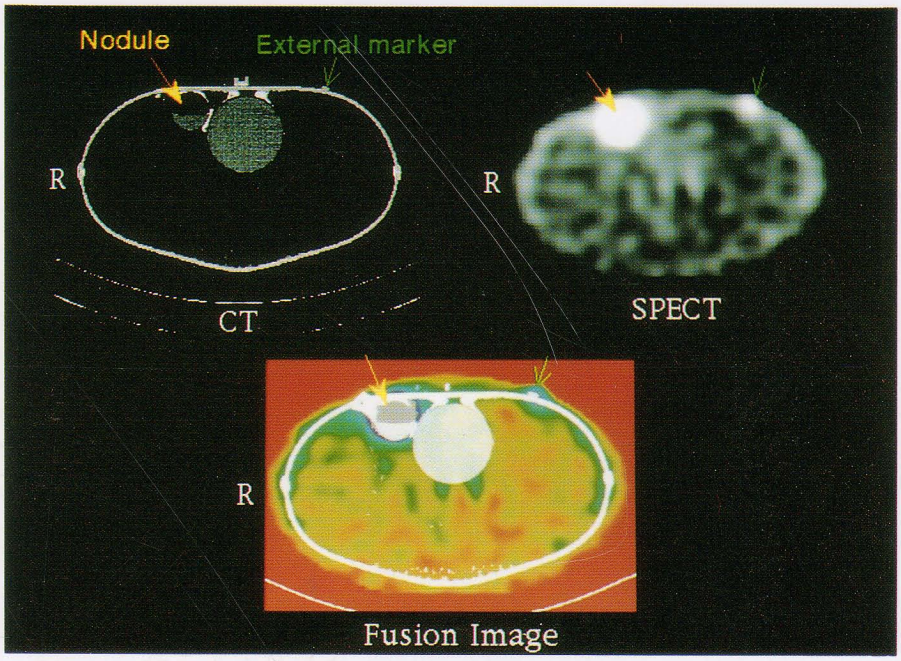

B

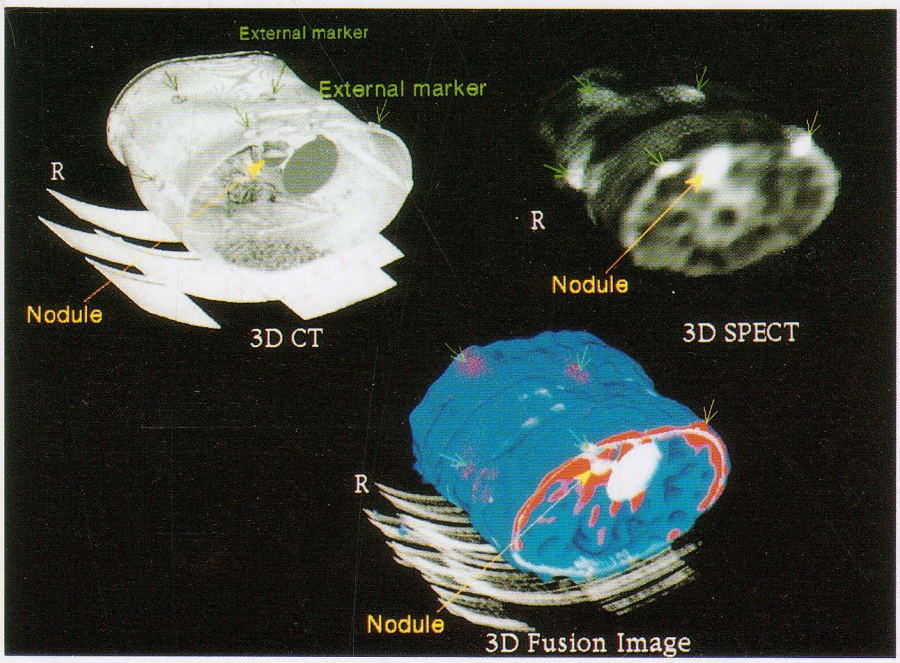

C

Fig. 4 (A) A photograph of a chest phantom with simulated lung nodule. The inside of this phantom contains a simulated mediastinal structure surrounded by the simulated lung structure filled with small styrenes foam. Radionuclide solution can be instilled to the simulated lung nodule through two-way silicon tubes (➡). Five external Tc-99m markers are also placed on the surface of this phantom (→). (B) CT transaxial 3-mm-thick slice image at the level of a simulated lung nodule (top; left) and reconstructed l-voxel-thick (3.2 mm) transaxial SPECT slice at the same level of CT slice (top; right), and the registered image of these CT and SPECT images at the level of a simulated lung nodule with radioactivity of Tc-99m (bottom). The Tc-99m-avid simulated lung nodule (yellow arrow) and surface markers (green arrow) are well matched on the registered image. (C) Three-dimensional images of CT (top; left) and SPECT (top; right), and a fusion image of these images (bottom). The fusion image well defines anatomic locations of the simulated lung nodule (yellow arrow) and surface markers (green arrows), which appear as the areas with the most intense activity of Tc-99m (reddish colors).

accuracy of the fit of the fusion image of CT and SPECT images of the chest phantom, the distances of the 5 surface markers, and the central and 7 peripheral points on the simulated lung nodule from the center or central line of each of the transaxial planes of this phantom were measured by multiplying the number of pixels in that distance by a 0.95 cm/pixel calibration factor (1 pixel = 0.95 cm, on the SPECT image acquired with the three-headed camera and transferred to the Macintosh computer), and were then compared to CT-measured dimensions (Table 1). Data from SPECT- and CT-measured dimensions were expressed as the mean ± standard deviation (SD), and the differences between the means for the groups were assessed with a paired Student's t-test. A p-value of less than 0.05 was regarded as significant.

RESULTS

The body contour, of a simple form of the cylindrical phantom, was clearly visualized throughout on each transaxial SPECT slice detecting the Compton-backscatter photons from the external Tc-99m source (Fig. 2), but in the complex form of the hexagonal phantom, the body outline was visually degraded, since the sharply concave surfaces were not well delineated (Fig. 3). The diameter of the cylindrical phantom measured on SPECT image ranged from 271 mm to 339 mm (n = 13, mean: 298.1 ± 20.8 mm), and the mean difference from the known diameters of this phantom was 3.1 ± 20.8 mm. The mean percent difference in these measurements was therefore 1.5%, with a range of −8.1% to 14.9%. There were, overall, no significant differences between SPECT dimensions and known diameters (N.S.). The maximal diameters of the hexagonal phantom measured on the SPECT image ranged from 200.0 cm to 260.0 mm (n =13, mean: 220.7 ± 18.8 mm), with a mean difference of −19. 2 ± 18.8 mm between the known diameters. The mean percent difference in these measurements was −5.4%, with a range of −16.2% to 16.6%. Here, there were significant differences between SPECT dimensions and known maximal diameters ($p < 0.01$).

The body outline of the chest phantom showed excellent correlation to the cylindrical phantom, and the concave and convex surfaces were clearly visualized (Fig. 4-B). With a 100 keV ± 25% energy window, the simulated lung nodule with Tc-99m activity was simultaneously visualized in this phantom. The comparison of the CT and SPECT dimension measurements in the registered image of the chest phantom is shown in Table 1. Twelve of the 13 measured dimensions on SPECT were greater than those measured on CT images. The dimension differences tended to be greater in the phantom portions with larger circumferences. The dimension differences in a total of 13 measurements ranged from −0.4 mm to 12.7 mm (mean: 6.8 ± 4.4 mm), and the mean percent difference was 5.0%, with a range of −0.5% to 12.0%. In the 8 measurements in the simulated lung nodule, dimension differences ranged from 2.3 mm to 7.1 mm (mean: 4.2 ± 1.5 mm), and the mean percent difference was 6.1%. SPECT-measured dimensions were, overall, significantly greater than CT measured dimensions ($p = 0.0001$). According to the resultant mean percent dimensional difference of 5.0% between the SPECT and CT phantom images, all registered transaxial SPECT images were uniformly minified by multiplying with a factor of 0.95 (1 − 0.05), and the registration with CT slices was re-performed. As a result, the dimension differences in the total of 13 measurements ranged from −3.9 mm to 6.4 mm (mean: 0.67 ± 3.3 mm), and the mean percent difference was reduced to 0.2%, with a range of −5.5% to 6.4%. In the 8 measurements of the simulated lung nodule, dimension difference ranged from −3.9 mm to 1.1 mm (mean: 0.8 ± 1.7 mm), and the mean percent difference wa reduced to −1.1%. There were, overall, no significant differences between SPECT- and CT-measured dimensions (N.S.). The body contour, each of the external surface markers, and the simulated lung nodule were visually well fitted on each of the transaxial slices of the registered image (Fig. 4B). The reconstructed 3-D fusion image well defined the anatomic locations of the simulated lung nodule and the surface markers (Fig. 4C).

DISCUSSION

This study demonstrated the feasibility of using external Tc-99m Compton scatter sources to obtain body-contour SPECT images of relatively simple forms of the cylindrical and chest phantoms. This method was also useful for creating a fusion image with SPECT and CT images of the chest phantom. In the created three-dimensional fusion image, target localization of the simulated lung nodule was accurately achieved with a mean alignment error of only 6.1%. In view of the relatively poor resolution of SPECT images compared to images from CT imaging, and the differences between those images in the acquisition matrix and slice thickness, this alignment error seems within acceptable limits for the validation of this method.

Body-contour SPECT images have been primarily used for attenuation corrections in quantitative SPECT studies, and a variety of methods using the object emission data either from photopeak[1–3] or Compton scatter windows,[4] 90° or backscatter Compton scatter photons from external sources,[5–8] surface markers,[9,10] and transmission SPECT data[11–14] have been proposed. Of these methods, the use of body surface markers including point or line sources, or internal anatomical landmarks and surface contours obtained from object emission data, either from photopeak or a Compton scatter window, have also been used for obtaining fusion images with CT images.[8,10] The method of using external Tc-99m Compton scatter sources has recently been used for a fusion image of CT and Bremsstrahlung SPECT images in patients treated with P-

32 therapy,[6–8] but, as shown in this study, this method may be applicable for creating fusion images of SPECT and CT images in routine clinical studies. It may also be the simplest technique since no special image processing is required, and the usual reconstruction methods can be used. Skin absorbed doses of radiation in patients are considered to be minimal, since radioactive sources are placed on the collimator rather than on the patient's skin. The dose of skin absorbed radiation has been estimated to be < 20/3 mrad for the 10 to 20 min required for projection images over 360° of rotation, with a 1 mCi source of Tc-99m at a mean distance of 10 cm from the skin surface of a subject.[5] In contrast, the method using body surface markers requires many radioactive sources all over the body surface to obtain high quality body-contour images, therefore increasing patient exposure to radiation, and it is also cumbersome. Because of the discontinuous body surface imaging obtained by this method, imaging quality is also apparently inferior to the present method and is not as clinically feasible.[14] The method which uses transmission CT data requires external radioactive plate sources, with a much greater dose of radionuclide. In addition, this method requires a SPECT scan twice, thereby increasing the dose of radiation absorbed by patients.[11–14] Internal anatomical landmarks and surface contour obtained from object emission data cannot be used when radiopharmaceuticals are used that accumulate in target specific tissues, but are not widely distributed throughout the organs or soft tissues of patients. The present method with the mixed Compton 90° or 180° scatter photons is simpler to perform than the Compton scatter technique reported by Macey et al.,[5] which required a collimated Tc-99m source and a secondary scatter window. A lower energy Compton scatter window other than Tc-99m could alternatively be used in the present method; for example, thallium-201, which has backscatter photons at 55–61 keV, but the use of thallium is not as practical as the use of Tc-99m.[7,8]

Clear visualization of the body contour and an accurate dimensioning with errors of only 1.5% in the SPECT images of the cylindrical phantom are consistent with those of similarly shaped phantoms evaluated by other investigators in attenuation correction and Bremsstrahlung SPECT studies.[5–7] Nevertheless, imaging quality and dimensions of the SPECT images of the complex hexagonal phantom were significantly degraded in this study. This degradation may be due to increases in the wide-ranging energies and directions of the Compton scatter photons from the sharply concave surfaces of this phantom. This method therefore may be inadequate for obtaining body contours of very complex forms of objects, but in routine SPECT studies elliptical human body portions, such as the abdomen and pelvis with genital concave and convex surfaces similar to the present chest phantom, are usually scanned. This limitation will therefore not interfere with the practical use of this method in clinical situations.

With a clear body-outline, the body contour SPECT image of the chest phantom simultaneously visualized the simulated lung nodule with Tc-99m activity, since the use of a 100 keV ± 25% energy window also detected some Compton scatter derived from the Tc-99m-avid lung nodule. Consequently, the three-dimensional fusion image with the CT image well visualized anatomical localization of this nodule. A fusion imaging with this method may therefore be useful for accurately localizing target tissue that accumulates Tc-99m-labeled tumor-seeking agents. But when using a radionuclide other than Tc-99m, such as thallium-201, gallium-67 citrate or Iodine-131 as a tumor-seeking agent, an additional SPECT scanning is needed to evaluate the tumor uptake of these tracers. Nevertheless, camera-computer systems capable of simultaneous acquisition of two windows of different photon energies will make the method easy and efficient to apply in routine clinical environments. Scatter from radionuclide within the target tissue is supposed to represent only a small fraction of the Compton scatter events detected from external sources, and so may not interfere with this method, but further study will be needed to evaluate this issue in relation to this method.

The accuracy of the fit between SPECT and CT images of the chest phantom, which was performed by visual inspection on the image matching soft ware, seems to be within acceptable limits, but a better fit was obtained after correction of the geometry of the body-contour SPECT images according to the calculated dimensional errors. Image registration by means of visual inspection alone may be greatly affected by the features and quality of SPECT images, and may inherently show some limitations of accurate body-contour matching. There are many factors causing geometric differences between CT and SPECT images. SPECT dimensions could be affected by acquisition matrices and slice thickness, and by reconstruction techniques including cutoff frequencies, reconstruction filters, and other pre- and postprocessing parameter changes.[7,8] Thresholds for imaging, and the full-width-at half-maximum (FWHM) of the SPECT system also affect SPECT dimensions.[13] As was demonstrated in the cylindrical phantom, some dimensional errors may already exist in the pre-registered SPECT images, even in a simple form object. Fully automatic quantitative registration techniques, therefore, are desirable to minimize geometric differences between SPECT and CT images. In the thoracic region, a respiration-gated imaging approach also should be followed to apply the present method in clinical use. Further study is still warranted to establish the most adequate technical approaches.

In conclusion, this phantom study showed the feasibility of a simple method, using Tc-99m Compton scatter sources to obtain body-contour SPECT images of a relatively simple form of an object, that avoided difficulties associated with surface radioactive markers. Although

further improvements in registration techniques are required, a body-contour SPECT image obtained by this method seems to have the potential to accurately create three-dimensional fusion images with CT images, without the need for internal landmark matching. These fusion images will be clinically helpful for accurately anticipating anatomical localization of a target tissue.

ACKNOWLEDGMENTS

This study was supported by Grant for Scientific Research No. 10670852 from the Japanese Ministry of Education.

REFERENCES

1. Berstrom M, Litton J, Eriksson L, et al. Determination of object contour from projection for attenuation correction in cranial positron emission tomography. *J Comput Assist Tomogr* 6: 365–372, 1982.
2. Webb S, Flower MA, Ptt RJ, Leach MO. A comparison of attenuation correction methods for quantitative single photon emission computed tomography. *Phys Med Biol* 28: 1045–1056, 1983.
3. Hosoda M, Wani H, Toyama H, Murata H, Tanaka E. Automated body contour detection in SPECT: Effects on quantitative studies. *J Nucl Med* 27: 1184–1191, 1986.
4. Jaszczak RJ, Chang LT, Stein NA, Moore FE. Whole-body single-photon emission computed tomography using dual large-field-of-view scintillation cameras. *Phys Med Biol* 24: 1123–1143, 1979.
5. Macey DJ, DeNardo GL, DeNardo SJ. Comparison of three boundary detection methods for SPECT using Compton scattered photons. *J Nucl Med* 29: 203–207, 1988.
6. Parsai EI, Ayangar KM, Dobelbower RR, Siegel JA. Clinical fusion of three-dimensional images using Bremsstrahlung SPECT and CT. *J Nucl Med* 38: 319–324, 1997.
7. Siegel JA, Zeiger LS, Order SE, Wallner PE. Quantitative Bremsstrahlung single photon emission computed tomographic imaging: use for volume, activity and absorbed dose calculations. *Int J Radiat Oncol Biol Phys* 31: 953–958, 1995.
8. Siegel JA. Quantitative Bremsstrahlung SPECT imaging: attenuation-corrected activity determination. *J Nucl Med* 35: 1213–1216, 1994.
9. Gullberg GT, Malko JA, Eisner RL. Boundary determination methods for attenuation correction in single photon emission computed tomography. *In* Emission Computed Tomography: Current Trends, Esser PD, ed., New York, The Society of Nuclear Medicine, pp. 33–53, 1983.
10. Larsson SA. Gamma camera emission tomography. *Acta Radiologica* 363 (suppl): 1–75, 1980.
11. Huang SC, Carson RE, Phelps ME, Hoffman EJ, Schelbert HR, Kuhl DE. Boundary method for attenuation correction in positron computed tomography. *J Nucl Med* 22: 627–637, 1981.
12. Maeda H, Ito H, Ishii Y, Mukai T, Todo G, Fujita T, et al. Determination of the pleural edge by gamma ray transmission computed tomography. *J Nucl Med* 22: 815–817, 1981.
13. Malko JA, Gullberg GT, Kowalsky WP, Van Heertum RL. A count-based algorithm for attenuation-corrected volume determination using data from an external flood source. *J Nucl Med* 26: 194–200, 1985.
14. Dey D, Slomka PJ, Hahn LJ, Kloiber R. Automatic three-dimensional multimodality registration using radionuclide transmission CT attenuation maps: A phantom study. *J Nucl Med* 40: 448–455, 1999.
15. Nishiyama Y, Wakimura K, Yamamoto Y, Takahashi K, Kawasaki Y, Satoh K, et al. I-123 SPECT-imaging with body outline using convenient lightweight source. *KAKU IGAKU (Jpn J Nucl Med)* 34: 119–125, 1997. (Japanese)